A High-Pressure Test of Birch's Law

A. J. Campbell and D. L. Heinz

The compressional wave velocities of polycrystalline NaCl and KCl have been measured to over 17 gigapascals, with the use of Brillouin scattering and the diamond anvil cell. This pressure corresponds to 40% compression for NaCl and 60% compression for KCl (including the volume change across the B1-B2 transition). The data obey Birch's Law, which predicts that the velocity of each material is linear with density, except across the B1-B2 phase transition in KCl. This deviation from Birch's Law can be rationalized in terms of an interatomic potential model wherein the vibrational frequencies of the nearest neighbor bonds decrease when going to the eight-coordinated B2 structure from the six-coordinated B1 structure.

The concept of velocity-density systematics has been critically important in geophysical research for over 30 years. Birch was the first to introduce this concept, in his seminal papers on the compressional wave velocities of rocks to 1 GPa (*1*), and as a result the relation:

$$V_P = a(\bar{m}) + b\rho$$

is known as Birch's Law, where V_P is the compressional wave velocity, ρ is the density, $a(\bar{m})$ is a parameter depending upon the mean atomic weight $\bar{m}$, and b is a constant. Birch hypothesized that this relation held when ρ was varied either by compression or phase transformation; thus, it is an ideal tool for construction of Earth models. At the time of Birch's original work the constraints on the density and composition of the Earth were the mass, moment of inertia, and the seismic velocities V_P and V_S (the subscript "S" refers to shear waves) versus Earth radius. Birch's Law allows one to calculate the density through the transition zone of the Earth, where the traditional Adams-Williamson approach fails because many silicates undergo phase transitions (*2, 3*). A form of Birch's Law has been recently used in seismic tomography to relate lateral changes in seismic velocities to changes in density, which are assumed to correspond to temperature differences (*4*). These models are used to place constraints on the flow patterns in the Earth's mantle (*5*). If the lateral velocity changes are related to compositional differences, then this use of Birch's Law is inappropriate.

Anderson (*6*) and later Shankland (*7*) generalized the velocity-density systematics to a power law formulation where the bulk sound speed is proportional to the density raised to some power. The change to bulk sound speed (or hydrodynamic velocity) from V_P was motivated by the desire to use a theoretical basis for their equations of state. Anderson's seismic equation of state is derived from interatomic pair potentials, while Shankland's formulation of velocity-density systematics is based upon Debye theory. In general there is a much better understanding of the bulk modulus compared to the shear modulus of solids; for instance, there are several formulations for the extrapolation of the bulk modulus as a function of pressure [the Birch-Murnaghan and Universal equations of state, for example (*8, 9*)], but most extrapolations of the shear modulus depend upon some form of Birch's Law. Because later formulations of velocity-density systematics involve the bulk sound speed and not V_P, we focus on Birch's Law.

We have measured V_P for polycrystals of NaCl and KCl to 17 GPa, using Brillouin spectroscopy with a diamond anvil cell (*10–14*), and used the data to test Birch's Law over a wide range of compression. NaCl and KCl were chosen because their high compressibilities allow large changes in density to be examined. In addition, KCl undergoes a structural phase transformation from the rock salt structure (B1) to the CsCl structure (B2) at 2 GPa; this transformation allows Birch's Law to be tested across a phase transition.

The Brillouin scattering experiments were performed on polycrystalline samples; in this way aggregate acoustic velocities were measured directly, and it was not necessary to average the individual elastic constants c_{ij} (*15–17*). Furthermore, higher pressures can be attained with polycrystalline specimens because there is no concern of bridging the sample between the diamond anvils or fracturing the sample under nonhydrostatic conditions; these problems have limited pressures attainable in single-crystal studies. Finally, we used a scattering geometry in which knowledge of the sample's refractive index is not required (*10*). Because of the low signal intensity of the shear wave velocities of the aggregate, we report only compressional wave velocities. The polycrystalline approach restricts sample selection to optically isotropic materials.

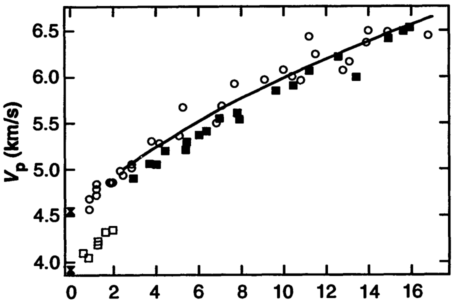

Fig. 1. Compressional wave velocity versus pressure. Open circles are NaCl (B1 structure), open squares are KCl (B1 structure), closed squares are KCl (B2 structure), and hourglass symbols are zero-pressure values. Data shown reflect several different polycrystalline samples of each composition. Solid line represents data of Frankel *et al.* (*18*). Pressure derivatives of V_P at zero pressure are 0.237 ± 0.003 km s^{-1} GPa^{-1} for NaCl and 0.29 ± 0.11 km s^{-1} GPa^{-1} for KCl.

The high-pressure results (Fig. 1), when extrapolated to 1 bar, are in good agreement with 1-bar values calculated from single-crystal elastic constants (4.55 km s^{-1} for NaCl and 3.92 km s^{-1} for KCl). Frankel *et al.* (*18*) reported ultrasonic measurements for polycrystalline NaCl to 27 GPa. Our Brillouin scattering measurements are in excellent agreement with their results (*19, 20*). P-wave velocities of all three phases investigated vary linearly versus density (Fig. 2), even over the large density increases involved (*21, 22*). These data lend validity to a linear velocity-density formu-

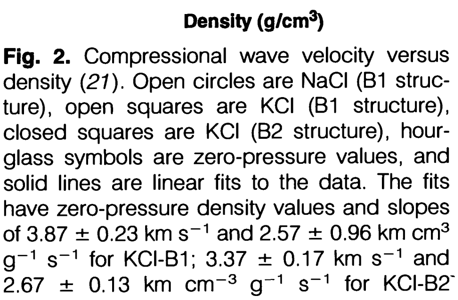

Fig. 2. Compressional wave velocity versus density (*21*). Open circles are NaCl (B1 structure), open squares are KCl (B1 structure), closed squares are KCl (B2 structure), hourglass symbols are zero-pressure values, and solid lines are linear fits to the data. The fits have zero-pressure density values and slopes of 3.87 ± 0.23 km s^{-1} and 2.57 ± 0.96 km cm^3 g^{-1} s^{-1} for KCl-B1; 3.37 ± 0.17 km s^{-1} and 2.67 ± 0.13 km cm^{-3} g^{-1} s^{-1} for KCl-B2 (excluding the outlier); and 4.525 ± 0.035 km s^{-1} and 2.616 ± 0.035 km cm^3 g^{-1} s^{-1} for NaCl-B1, respectively.

A. J. Campbell, Department of the Geophysical Sciences, University of Chicago, Chicago, IL 60637.

D. L. Heinz, Department of the Geophysical Sciences and James Franck Institute, University of Chicago, Chicago, IL 60637.

lation in the cases of NaCl and KCl, for a single phase.

Although linear velocity-density trends are observed within one phase, Birch's Law does not appear to hold through a structural phase transition (*23*). The compressional wave velocity of KCl is seen to be discontinuous over the B1-B2 phase transformation (Fig. 2). The slopes of the velocity-density trends are similar for the high-pressure and low-pressure phases of KCl, but the compressional wave velocity of the high-pressure phase is ~0.50 km s^{-1} lower than would be predicted by extrapolation from the low-pressure phase, according to Birch's Law. This effect had been anticipated by Jeanloz (*24*) on the basis of interatomic potential models of coordination changes induced by a phase transition. Jeanloz (*24*) argued that a decrease in vibrational frequencies should be associated with the increasing bond distance across the transition from the B1 to the more highly coordinated B2 structure; this frequency decrease is reflected in the acoustic velocities. Continuum-based theories of velocity-density systematics [for example, Birch's Law and Anderson's (*6*) seismic equation of state] do not predict this behavior (*24*).

In most of the earlier applications of Birch's Law to the deep interior of the Earth, it was assumed that the relation was applicable to changes in density caused by compression, temperature, and phase transitions. The simple linear relation between compressional wave velocity and density underlines the importance of density or volume on controlling the thermodynamic properties (*1*, *3*, *6*). If bulk modulus measurements of a material as a function of temperature are corrected back to the initial volume, the corrected bulk moduli are insensitive to temperature (*25*). Thus, the bulk sound speed formulations of velocity-density systematics (which depend only on the bulk modulus) should work for variations in velocity due to temperature variations. This effect is in contrast to Birch's Law (which depends on both the bulk and shear moduli), where we expect to see an intrinsic temperature effect because the shear moduli are sensitive to temperature even when they are corrected to constant volume (*25*). Thus, care should be taken in applying Birch's Law to velocity changes induced by temperature variations.

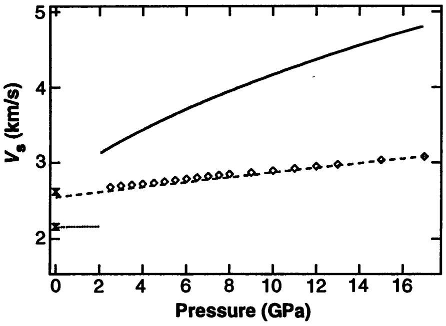

Fig. 3. Shear wave velocity versus pressure. Shear wave velocities are calculated from fits to the compressional wave velocity-density curves in Fig. 2 and isothermal equations of state. Dashed line is NaCl (B1 structure), dotted line is KCl (B1 structure), and solid line is KCl (B2 structure). Diamonds are data from Frankel *et al.* (*18*), and hourglass symbols are zero-pressure values. Measured zero-pressure values of V_S are 2.54 km s^{-1} for NaCl and 2.15 km s^{-1} for KCl, with pressure derivatives at zero pressure of 0.035 km s^{-1} GPa^{-1} for NaCl and 0.015 km s^{-1} GPa^{-1} for KCl.

Although shear wave scattering in these polycrystalline samples was not of sufficient intensity to allow measurement by our Brillouin scattering apparatus, we can calculate S-wave velocities from the data on compressional wave velocity by incorporating the density and bulk modulus values from the isothermal equations of state (*8*, *22*) and including a small isothermal-to-adiabatic correction to the bulk modulus. The relation between P-wave velocity and S-wave velocity is

$$\rho V_P^2 = K_S + \left(\frac{4}{3}\right)\rho V_S^2$$

where V_S is shear wave velocity and K_S is the adiabatic bulk modulus. The V_S (see Fig. 3) values obtained in this way compare well with 1-bar data (2.62 km s^{-1} for NaCl and 2.16 km s^{-1} for KCl). This treatment of the V_P data is rather sensitive to the equation of state used. An interesting feature shown in Fig. 3 is the relatively small pressure derivatives of V_S in the rock salt structured phases compared to the CsCl structure of KCl; this behavior may reflect the presence of phase transitions at 2 GPa for KCl and 29 GPa (*26*) in NaCl.

REFERENCES AND NOTES

1. F. Birch, *J. Geophys. Res.* **65**, 1083 (1960); *ibid.* **66**, 2199 (1961).
2. E. D. Williamson and L. H. Adams, *J. Wash. Acad. Sci.* **13**, 413 (1923).
3. F. Birch, *J. Geophys. Res.* **69**, 4377 (1964).
4. A. M. Dziewonski, B. H. Hager, R. J. O'Connell, *ibid.* **82**, 239 (1977); B. H. Hager, R. W. Clayton, M. A. Richards, R. P. Comer, A. M. Dziewonski, *Nature* **313**, 541 (1985).
5. B. H. Hager and R. W. Clayton, in *Fluid Mechanics of Astrophysics and Geophysics*, W. R. Peltier, Ed. (Gordon and Breach, New York, 1989), vol. 4, pp. 657–763.
6. D. L. Anderson, *Geophys. J. R. Astron. Soc.* **13**, 9 (1967).
7. T. J. Shankland, *J. Geophys. Res.* **77**, 3750 (1972).
8. F. Birch, *ibid.* **83**, 1257 (1978).
9. P. Vinet, J. Ferrante, J. H. Rose, J. R. Smith, *ibid.* **92**, 9319 (1987).
10. Polycrystalline NaCl (Alfa, lot. no. 082085) and KCl (Alfa, lot no. 073184) were loaded into a Merrill-Bassett–type diamond anvil cell with sapphire diamond supports (*11*), using a stainless-steel gasket. The diamonds were one-quarter carat with 250-μm culets; samples were ~100 μm in diameter. A few small grains of ruby were placed into the sample chamber for the ruby-fluorescence pressure measurement (*12*). Care was taken to ensure that a ruby chip could always be found near the probed portion of the sample; errors in the pressure measurement are estimated at 3%, with a minimum of 0.1 GPa. Numerous samples of both KCl and NaCl were used. Details of the Brillouin-scattering process and standard experimental techniques are in (*13*). A single mode from the 514.5-nm line of an Ar$^+$ laser provided the incident light for the Brillouin scattering measurements. Scattered light was collected at 90° from the incident beam and was passed through a five-pass Fabry-Perot interferometer before detection. A Burleigh DAS-1 data acquisition system was used to record the photomultiplier tube signal as well as maintain alignment of the interferometer. The geometry used by Whitfield *et al.* (*14*) was adopted for these experiments. In this arrangement both the incident and scattered light describe a 45° angle with the diamond cell axis, and the phonon wavenumber (q) is constrained, independent of the sample's index of refraction, as $q = 1.414\ k_L$ (where k_L is the wavenumber of incident light in vacuum). It is important in this geometry that interfaces between materials with different indices of refraction (between sample, diamond, sapphire, and air) remain parallel; compliance with this requirement was verified through reflection of a laser beam off of both sides of the cell. Constraints upon the sample geometry prohibit the introduction of a pressure-transmitting medium with polycrystalline samples. We therefore minimized the possible effect of pressure gradients on these measurements by probing only a small (~15 μm) spot at the center of the sample chamber. Positions of the Brillouin and Rayleigh peaks in the 512-channel spectrum were precisely determined by fitting each peak to a Gaussian profile. The total frequency shift between two Rayleigh peaks (the free spectral range), which is governed by the spacing of the interferometer plates, was calibrated with an acetone standard and several lines of an Ar$^+$ laser (excluding 514.5 nm). The free spectral range was carefully set to avoid overlap of Brillouin peaks from the diamond with those from the sample. An acousto-optic modulator was used to attenuate the incident laser light while the Rayleigh peaks were being recorded.
11. R. M. Hazen and L. W. Finger, *Comparative Crystal Chemistry: Temperature, Pressure, Composition and the. Variation of Crystal Structure* (Wiley, New York, 1982).
12. H. K. Mao, P. M. Bell, J. W. Shaner, D. J. Steinberg, *J. Appl. Phys.* **49**, 3276 (1978).
13. L. Brillouin, *Ann. Phys.* (*Paris*) *9th Ser.* **17**, 88 (1922); D. J. Weidner, *Geophys. Res. Lett.* **2**, 189 (1975); ——— and H. R. Carleton, *J. Geophys. Res.* **82**, 1334 (1977); M. Grimsditch and A. Polian, in *Simple Molecular Systems at Very High Density*, A. Polian, P. Loubeyre, N. Boccara, Eds. (Plenum, New York, 1989), pp. 237–255.
14. C. H. Whitfield, E. M. Brody, W. A. Bassett, *Rev. Sci. Instrum.* **14**, 942 (1976).
15. The single crystal elastic constants for any material that is elastically anisotropic (cubic or lower symmetry) need to be averaged to obtain the isotropic values. This averaging process results only in bounds being placed upon the isotropic elastic moduli (*16*). Grain size effects should also be considered in investigations of polycrystalline material. Typical grain size of the NaCl and KCl powders before pressurization was estimated to be 1 to 2 μm. Because this grain size is much larger than the phonon half-wavelength (182 nm), the Brillouin signal recorded is actually a summation of Brillouin-scattered light from many different crystallites, each with arbitrary orientation. In this way, all crystallographic directions are implicitly averaged in the polycrystal, and the measured Brillouin shift corresponds to the aggregate wave velocity. This reasoning is identical to that used by Yeganeh-Haeri *et al.* (*17*) in their Brillouin scatter-

ing study of aggregate garnets. With the incident laser beam focused to a spot size of 15 μm and a scattering length in the sample of only 15 μm at high pressures, even an average grain size of 2 μm results in several hundred randomly oriented crystallites being probed during the experiment. This ensures that an appropriate orientational average is being sampled.
16. J. P. Watt, G. F. Davies, R. J. O'Connell, *Rev. Geophys. Space Phys.* **14**, 541 (1976).
17. A. Yeganeh-Haeri, D. J. Weidner, E. Ito, *Geophys. Res. Lett.* **17**, 2453 (1990).
18. J. Frankel, F. J. Rich, C. G. Homan, *J. Geophys. Res.* **81**, 6357 (1976).
19. The P-wave velocity data set was obtained independently of earlier results; Frankel *et al.* (*18*) relied on the isothermal equation of state of NaCl to estimate the sample thickness, a necessary parameter in the data reduction of their ultrasonic technique. Pressures are also measured more precisely with the ruby-fluorescence technique used in our work; Frankel *et al.* (*18*) estimated an error of ±15% from their resistometric calibration. Birch (*8*) compared the high-pressure polycrystalline NaCl results of Frankel *et al.* (*18*) with those of Morris *et al.* (*20*) (to 9 GPa) and those of Voronov and Goncharova (20) (to 10 GPa) and found very good agreement among these data sets using ultrasonic techniques; this work is further verified by the results of our Brillouin-scattering experiments. However, as Birch (*8*) pointed out, there remains some discrepancy between the zero-pressure slopes inferred from high-pressure polycrystalline work and low-pressure single crystal work; this issue needs further clarification.
20. C. E. Morris, J. C. Jamieson, F. L. Yarger, *J. Appl. Phys.* **47**, 3979 (1976); F. F. Voronov and V. A. Goncharova, *Soviet Physics JETP* **23**, 777 (1966).
21. To calculate density as a function of pressure, isothermal equation of state data were taken from Birch (*8*) for NaCl, Yagi (*22*) for the low-pressure (B1) phase of KCl, and Campbell and Heinz (*22*) for the high-pressure (B2) phase of KCl.
22. A. J. Campbell and D. L. Heinz, *J. Phys. Chem. Solids* **52**, 495 (1991); T. Yagi, *ibid.* **39**, 563 (1978).
23. R. C. Liebermann and A. E. Ringwood, *J. Geophys. Res.* **78**, 6926 (1973).
24. R. Jeanloz, in *High-Pressure Research in Geophysics*, S. Akimoto and M. H. Manghnani, Eds. (Center for Academic Publications Japan, Tokyo, 1982), vol. 12, pp. 479–498.
25. D. C. Wallace, *Thermodynamics of Crystals* (Wiley, New York, 1972).
26. Y. Sato-Sorensen, *J. Geophys. Res.* **88**, 3543 (1983).
27. The technical assistance of M. Vaughan and M. Grimsditch is gratefully acknowledged. D. Anderson and two reviewers provided valuable comments on the manuscript. This work was supported by National Science Foundation grant EAR-9104885 and the Materials Science Laboratory at the University of Chicago.

6 April 1992; accepted 29 May 1992

Chemiluminescence of Anodized and Etched Silicon: Evidence for a Luminescent Siloxene-Like Layer on Porous Silicon

Paul McCord, Shueh-Lin Yau, Allen J. Bard*

Treatment of anodized or chemically etched silicon ("porous silicon") with dilute nitric acid or persulfate solution results in weak chemiluminescence in the visible region. Concentrated nitric acid reacts violently with porous Si produced by anodization with a bright flash of light. The fact that similar reactions occur with siloxene ($Si_6H_6O_3$) prepared from $CaSi_2$ suggests that the visible emission seen with porous Si can be attributed to this substance.

Recent interest in porous Si and very small Si particles largely arises from the photoemission in the visible region observed with these materials, indicating a radiative transition well above the indirect band gap of bulk crystalline Si (*1–7*). This effect has been attributed to the presence of nanometer-size Si structures (Q-particles and quantum dots or wires) in which quantum-size effects (*1*, *2*) occur. However, an alternative explanation for this emission is the alteration of the composition of the Si upon anodization or etching which produces new Si-based compounds that luminesce at visible wavelengths. For example, recent work by Brandt *et al.* (*6*) has demonstrated that the photoluminescence and vibrational spectra of porous Si can be attributed to siloxene derivatives. In this report we show that treatment of porous Si with nitric acid or persulfate can result in chemiluminescence, as occurs with siloxene prepared from $CaSi_2$. These results strongly suggest that the luminescence of porous Si is attributable mainly to formation of siloxene-like compounds.

Porous Si was prepared by two different methods. In the first, single-crystal polished *p*-type Si (100) wafers (1 ohm-cm) were anodized in a solution of hydrofluoric acid (HF), acetic acid (CH_3COOH), and ethanol (1:1:1), as previously described (*8*). In the second, the Si wafer was chemically etched with a solution of HF, HNO_3, CH_3COOH, and H_2O (1:2:1:4) for 5 to 10 min (*7*). The resulting porous Si, formed by either method, ranged from a dull yellowish-brown to a darker brown in color and showed the characteristic bright orange to red luminescence when illuminated with an ultraviolet (UV) source (Mineralight UVGL-25).

When a piece of porous Si was immersed in an ~4 M HNO_3 solution, a weak chemiluminescence was observed that could be imaged with a charge-coupled device (CCD) camera (Model CH210, Photometrics, Tucson, Arizona) cooled to −113°C (Fig. 1A). Porous Si in contact with HNO_3 vapor also produced chemiluminescence. Figure 1B is an image of the same piece of porous Si as shown in Fig. 1A but with the sample suspended ~0.5 cm above the HNO_3. This chemiluminescence probably arises from the reaction between the porous Si and the NO_2 gas present in the vapor phase. Chemiluminescence generated in the vapor phase was passed through a monochromator (Model 100S, American Holographic, Littleton, Massachusetts) and the resulting spectrum (imaged with the CCD) (Fig. 2) also shows the photoluminescence of the same piece of porous Si in air illuminated by a hand-held UV lamp (370-nm excitation).

The chemiluminescence obtained from the HNO_3 solution slowly decayed to about one-half of its original brightness in 10 min. Note that the chemiluminescence in either the liquid or gas phase was very weak and was not visible to the eye in the

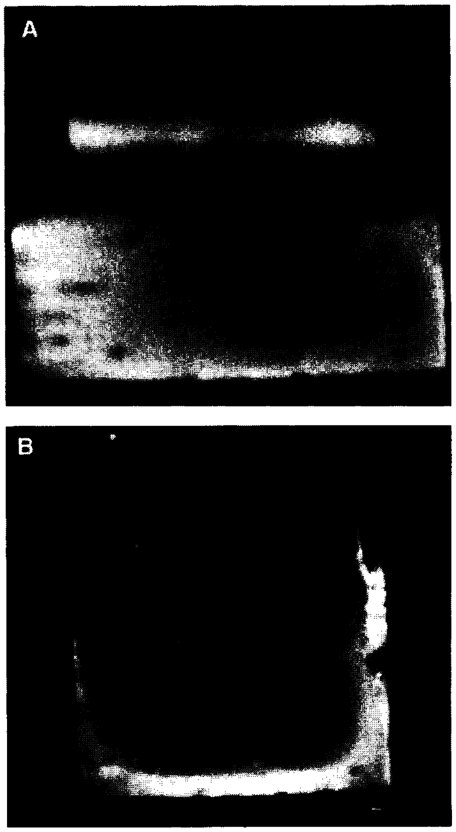

Fig. 1. (**A**) Porous Si immersed in an ~4 M HNO_3 solution. (**B**) Porous Si in the vapor phase above a concentrated HNO_3 solution.

Department of Chemistry and Biochemistry, the University of Texas at Austin, Austin, TX 78712.